# An Experimental Study of Permeability and Fluid Chemistry in an Artificially Jointed Marble

CHRIS MARONE AND JAMES RUBENSTONE

*Lamont-Doherty Geological Observatory and Department of Geological Sciences, Columbia University*

*Palisades, New York*

TERRY ENGELDER

*Department of Geosciences, Pennsylvania State University, University Park*

To examine the amount of rock dissolution accompanying changes in joint permeability, deionized water was forced through axially split cylindrical samples of Vermont marble, subjected to a confining pressure of 60 MPa. Surface preparation and loading conditions varied among experiments during which permeability and fluid chemical composition were monitored with time. Time dependent permeability and fluid composition for freshly polished joints differed from joints which had been "etched" by the fluid during previous runs. For freshly polished surfaces, permeability decreased and fluid chemical concentrations increased during the first 50 to 100 hours of fluid flow. For the water-etched surfaces, permeability was not time dependent, and a steady state chemical composition was reached after 20 to 40 hours. A calculation of the steady state chemical concentrations for coexisting calcite and dolomite in deionized water, at a fluid pressure of 10 MPa and a confining pressure of 60 MPa, shows that the steady state values reached in our experiments were supersaturated. Supersaturation was probably due to enhanced solubility at contact points together with precipitation inhibition. Our data indicate that fluid flow through fresh fractures causes dissolution of contact points and permeability reduction, depending on the morphology and state of the fracture surfaces.

## INTRODUCTION

Significant volume loss commonly accompanies deformation within at least the upper 10 km of the crust [*Wright and Platt*, 1982; *Engelder*, 1984; *Etheridge et al.*, 1984]. In many cases the volume loss appears as a mass transport of rock over distances in excess of 1 to 10 km. Given the limited solubilities of most rock-forming minerals under crustal conditions, mass transport of large rock volumes ($\approx$ 10 to 50% of a deforming formation) requires circulation of very large fluid volumes along networks of interconnected joints and shear fractures. One mechanism for reducing the volume of water necessary for mass transport is through supersaturation of the circulating fluid. In this paper we examine the degree of supersaturation arising from the dissolution of rock along joints forced together under high normal stress.

Within the upper crust, joint aperture and hence permeability are controlled by grain-scale deformation mechanisms, which include the physicochemical reactions that occur when a stressed solid reacts with a flowing solvent [*Bathurst*, 1958; *Weyl*, 1959; *Robin*, 1978; *Fyfe et al.*, 1978]. Within joints, these reactions cause permeability changes via dissolution and redistribution of the material at contact points or within flow channels. The process of stress-enhanced dissolution and material redistribution is commonly called pressure solution [e.g., *McClay*, 1977]. Since the permeability of jointed rocks is strongly dependent

on the effective hydraulic aperture of the joints [e.g., *Iwai*, 1976], pressure solution within joints will have a major influence on the bulk transport properties of rocks.

Time dependent permeability of joints within rocks depends on the kinetics of dissolution/precipitation reactions and fluid flow rates. The extent to which joint permeability is controlled by these latter factors depends upon the accessibility of fluid to solid-solid contact areas and the effect of flow rate on dissolution and precipitation. The mechanism of fluid access and subsequent dissolution under contact areas differs among models for pressure solution [*Bathurst*, 1958; *Weyl*, 1959; *Robin*, 1978; *Rutter*, 1983; *Tada and Siever*, 1986]. Two basic mechanisms have been proposed. One model [*Weyl*, 1959] proposes that asperities are removed through dissolution and diffusion along an adsorbed layer which is present within solid-solid contact areas. The second model [*Bathurst*, 1958] proposes that dissolution occurs in areas adjacent to high-stress contact points and that stepwise crushing occurs when the contact area is reduced to a critical size. Depending on which of these mechanisms is dominant in a given system, dissolution may lead to reduction of the joint aperture and permeability reduction, or, possibly, permeability increase via dissolution within cavities and flow channels. To date, experimental data on permeability changes for isothermal isobaric conditions are sparse [e.g., *Kranz and Blacic*, 1984]. Related work on permeability changes in a temperature gradient shows large permeability changes due to precipitation of material at the low-temperature end of the sample [*Summers et al.*, 1978; *Morrow et al.*, 1981; *Moore et al.*, 1983].

The experiments reported here are an attempt to identify the relationship between dissolution and permeability along a rock joint through which a solvent for the rock is flowing.

Because surface polishing of the samples prior to an experiment has a poorly understood effect on initial dissolution [e.g., *Chave and Schmalz*, 1966; *Holdren and Berner*, 1979; *Sass et al.*, 1983; *Walter and Morse*, 1984; *Chou and Wollast*, 1984], we have varied surface preparation in these experiments. The initial roughness of the joint surfaces was maintained constant during this series of experiments in order to isolate the effects of polishing. The effects of applying a normal load across the joint surface at the beginning of an experiment were considered by comparing experiments with and without load cycling prior to the initiation of fluid flow tests.

## EXPERIMENTAL TECHNIQUE

Experiments ranged in length from a few days to 3 weeks and were conducted in a servocontrolled triaxial apparatus capable of continuous fluid flow through samples subjected to confining pressures of up to 600 MPa and ambient fluid pressures up to 200 MPa. All experiments were run at 25°C. The confining pressure $(P_c)$ was maintained constant to within 5% over the course of experiments using an Argon gas confining medium. Axial load was measured with an external load cell in series with the loading piston. Pressures are accurate to within 1%. The differential fluid pressure over the sample length $(\Delta P_f)$ and the average fluid pressure within the joint $(P_f)$ were independently controlled via two high-pressure piston cylinders connected to the top and bottom of the sample, respectively (reservoirs A and B, Figure 1). A change in flow direction occurred when the high-pressure-side $P_f$ piston advanced to a preset displacement limit; occasionally, these changes were imposed manually. At that point, the direction of the hydraulic gradient across the sample was reversed. Fluid flow rates were derived from piston displacements, which were measured with linear variable differential transformers (LVDTs). A volume of $10^{-4}$ cm$^3$ could be resolved. The fluid used for the rock-water interaction was Millipore deionized water. The water was open to the atmosphere prior to use in an experiment, and thus, presumably, $P_{CO_2}$ was $10^{-3.5}$ atm.

Short-term variations in pressures during an experiment are given by the "deadbands" in the servocontrol systems. These are the pressure changes that can occur without a corrective response from the servocontrol system. They are, 0.1, 0.05, and 0.5 MPa for confining pressure, fluid pressure, and axial load, respectively. Short-term variations in the differential fluid pressure are therefore ± 0.1 MPa due to pressure variations within each fluid reservoir. Long-term drift in the fluid pressure transducers resulted in variations of the differential fluid pressure of up to ± 0.2 MPa over the course of an experiment.

The rock used in this study was Vermont marble, collected near Rutland, Vermont. This marble is composed of 65-70% calcite (grain size 80-150 μm), 25-30% dolomite (grain size 200-1000 μm), and 2-3% quartz and opaques (grain size 8-20 μm). Microprobe analysis of the calcite and dolomite yielded Ca/Mg molar ratios of 80 and 1.3, respectively (i.e., the dolomite composition is $Ca_{0.565} Mg_{0.435} CO_3$). Thus, the bulk Ca/Mg molar ratio for the rock is 5.97. The permeability of intact Vermont marble was measured to be $10^{-15}$ cm$^2$ at 50 MPa effective normal stress ($\sigma' = P_c - P_f$).

The rock samples used in these experiments were axially split cylinders 3.49 cm in diameter and 7.34 cm in length.
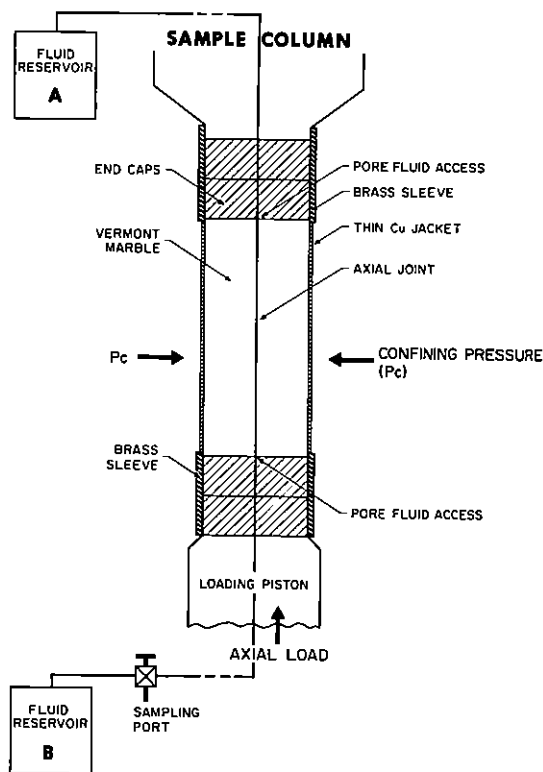


Fig. 1. Sample column assembly. Fluid was cycled through the sample from two reservoirs. The fluid reservoirs were made of 17-4-PH stainless steel and were connected to the sample by ≈1 m of high-pressure 316 stainless steel tubing. The piston, closure, and end caps were 17-4-PH stainless steel. The end cap in contact with the sample was grooved radially and circumferentially so as to disperse fluid over the entire sample end. The sample was soldered to the brass sleeves to effect a seal, and the sleeves were silver soldered to the closure and piston.

Artificially jointed cylinders were prepared by starting with rectangular blocks surface-ground flat to ± 0.0002 mm/mm. Two blocks were clamped together, and split cylinders were cut using a core bit centered on the seam between the blocks. The split-cylinder faces were then polished with successively finer grit to the desired finish. In these experiments, opposing surfaces of the split cylinder had different roughnesses: one surface finished with 400-grit silicon carbide polishing compound, the other with 0.3-μm alumina. The different roughnesses were intended to provide a fairly low permeability and to focus changes in asperity height and surface morphology on one surface. Following surface preparation, profiles were taken across the 400-grit surface, at 5-μm intervals, with a conical, 13-μm tip radius, stylus profilometer. The rms roughness of the 400-grit surfaces was 3.4 μm ± 0.1 μm.

After polishing, each sample half was washed individually in an ultrasonic bath of deionized water to remove the polishing compound and loose fragments. Three 15-min interval washes were done, between which the 250-mL bath was rinsed and refilled with clean deionized water. In two experiments, EDB-38 and EDB-30, the surfaces were further cleaned by placing the samples in a 150-mL solution of 5% HF and 0.1 N $H_2SO_4$ for 30 min to further remove loose and surface-damaged rock. Following the acid bath the samples were rinsed with deionized water. After the cleaning, the

samples were jacketed with a single 0.075-mm-thick layer of Cu foil and sealed within the sample column by soldering the Cu jacket to a brass sleeve (Figure 1).

Prior to an experiment, a nonreactive tube was installed in the sample column in place of the rock sample, and the fluid system (including the two fluid reservoirs) was flushed. This was done in order to establish the background levels of chemical species within the fluid system. Flushing consisted of cycling $\approx$ 65 cm$^3$ of deionized water through the $P_f$ system for between 15 and 20 hours, during which time the fluid was sampled for chemical analysis. Values for Ca and Mg are given in Figures 2 and 7, labeled "blank." In addition, we measured the concentrations of Fe, Si, Mn, Na, K, and Al in these fluids. The maximum values obtained in 20 hours of interaction with the fluid pressure system were, in moles per liter: Fe =7.22 x10$^{-7}$, Si =6.23 x10$^{-6}$, Mn =5.67 x10$^{-6}$, Na =6.22 x10$^{-6}$, K =1.28 x10$^{-5}$, and Al =1.85 x10$^{-6}$. Fe was also measured in fluid samples throughout the experiments to check for iron oxide precipitates and colloidal ferric oxides [e.g., *Potter et al.*, 1981]. The Fe values were typically between 8.95 x10$^{-6}$ and 1.79 x10$^{-5}$ mol/L (0.5 to 1 ppm by weight) after 100 to 200 hours of interaction. Therefore, based on the estimates of Potter et al., who found permeability reduction for Fe concentrations of 10 ppm or more, it is unlikely that colloidal iron or iron precipitates caused permeability reduction in the experiments reported here.

Immediately following the fluid system flush, the jacketed rock sample was installed in the vessel and loaded to 50 MPa with the confining pressure ($P_c$) maintained equal to the axial load ($\sigma_1$). The fluid system was then filled by pumping in 65 cm$^3$ of deionized water from a reservoir open to the atmosphere. After saturation of the rock, the fluid pressure was brought to 10 MPa, and air was bled from the $P_f$ system. $P_c$ and $\sigma_1$ were then raised to 60 and 120 MPa, respectively. (The axial load was measured with a load cell that was external to the pressure vessel. A differential stress was used to ensure that a tight seal was maintained between end caps within the sample column (see Figure 1) and that piston/seal friction was overcome.) The application of a differential fluid pressure of between 0.5 and 6.5 MPa, over the length of the sample, initiated flow through the rock; average $P_f$ remained 10 MPa.

Fluid was sampled periodically during an experiment, in 4-cm$^3$ aliquots, through a port between the rock and reservoir B. The fluid volume therefore decreased during an experiment as samples were taken. Fluid samples were acidified by addition of HCl (to 1 N solution) to inhibit precipitation after removal from the system. All of the samples taken during the series of 11 experiments were visibly clear when collected, and they were not filtered prior to chemical analysis. Fluid samples were analyzed for dissolved metals by direct-current plasma emission spectrometry using standard solutions that bracketed the observed concentrations. Precision and accuracy of the measurements are within ± 3%, based on replicate analyses.

Because the flow rate along the joint, typically 10$^{-3}$ to 10$^{-5}$ cm$^3$/s, was slow relative to the fluid sampling rate (about 1 cm$^3$/s), >99% of the fluid collected for chemical analysis was drawn from that which was already in reservoir B. This presented a problem, since fluid that had just passed through the joint was diluted by fluid already in reservoir B. The problem was most significant at the beginning of an experiment when the fluid in reservoir B was "fresh" deionized water. To minimize this problem, flow was always initiated from reservoir A to B, and the initial fluid in reservoir B was kept at 1-2 cm$^3$. The dilution caused by the unreacted fluid was then 6% or less after 33 cm$^3$ of fluid had passed through the sample, and this point is marked in the figures that follow. An additional problem was related to sampling from only one side of the joint (see Figure 1). This was done for reproducibility in sampling and to minimize the potential for contamination of fluid samples. However, this procedure introduces the potential for a stepwise approach to a steady state chemical composition, since the fluid in reservoir B does not change composition during flow from B to A (assuming the solute diffusion rate within the fluid system is slow relative to the flow rate). Effects of this sampling procedure are notable during the early portions of some experiments, as discussed later. Finally, because the fluid was not always in contact with the rock and because the fluid was sampled from only one reservoir (without being mixed with the entire fluid volume), the time required to reach a steady state chemical composition was flow rate dependent. That is, at sufficiently slow flow rates, the fluid exiting the joint would have already reached a steady state composition on its first pass. In this case, the time required to reach a steady state chemical composition as measured by our sampling procedure would be controlled by dilution with the fluid in reservoir B. At higher flow rates, fluid exiting the joint would not be at steady state, and thus several passes through the joint would be necessary before a steady state composition was reached. The transition between these regimes is controlled by the dissolution rate of the solid. These effects are noted in the figures that follow.

The fluid flow rate ($q$) was recorded continuously during an experiment and permeability ($\kappa$) was calculated using Darcy's law: $q = \kappa (A/\mu) (dP/dl)$, where $A$ is the cross-sectional area perpendicular to flow, $\mu$ is the viscosity of the fluid, and $dP/dl$ is the fluid pressure gradient over the length of the sample. We use the entire cross-sectional area of the sample, perpendicular to the cylinder axis, to calculate the permeability values reported in this paper.

## EXPERIMENTAL RESULTS

In order to elucidate the effects of surface polishing on permeability changes and chemical interaction, we distinguish two types of experiments based on the treatment of the joint surfaces prior to a run. In the first type, joint surfaces were polished and ultrasonically cleaned, as described above, immediately prior to the experiment. The only contact these samples had with fluid prior to an experiment was during polishing and subsequent cleaning. These experiments are labeled PW: polished and washed. In the second type of experiment, a sample was used consecutively from one run to the next without being removed from the vessel and, hence, without the surfaces being repolished or otherwise treated between runs (labeled RFx: run for $x$ hours prior to that experiment). During the course of an experiment, fluid was cycled back and forth through a sample from two fluid reservoirs. Except where otherwise noted, average fluid pressure ($P_f$), confining pressure ($P_c$), and axial load ($\sigma_1$) were held at 10, 60, and 120 MPa, respectively.
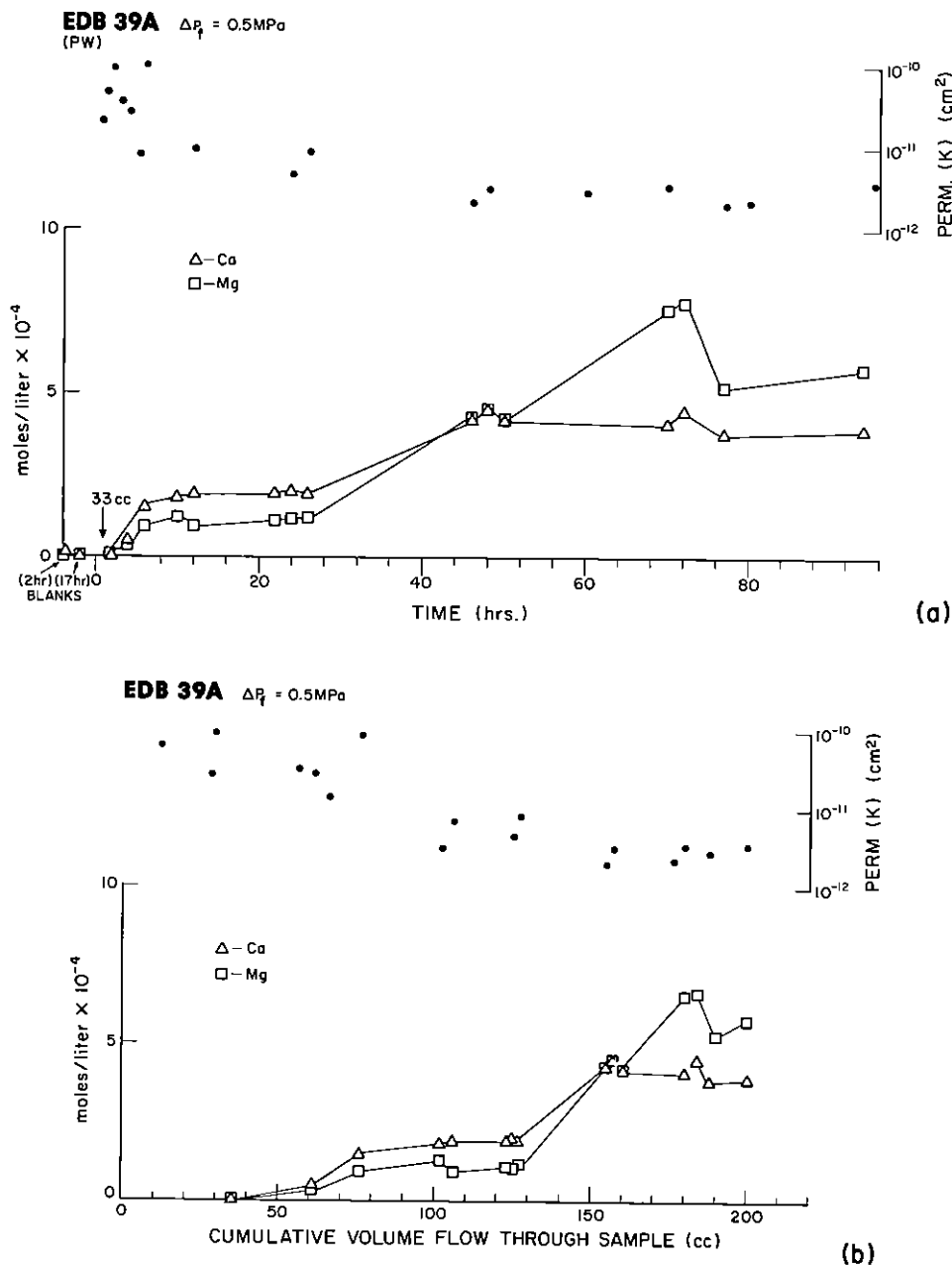
Fig. 2. Test EDB-39A. No initial acid cleaning was done following the polish and wash. Chemical "blanks" represent background levels of chemical species within the pore fluid system at the initiation of an experiment, without a rock sample, after flushing for 2 and 17 hours. (a) Permeability (circles) and chemical concentration (squares and triangles) versus time for a freshly polished sample (PW) are shown. Permeability decayed during the first 50 hours, after which it reached a steady state level. A chemical steady state was reached at between 50 and 60 hours. (b) The data from Figure 2a are plotted versus the cumulative volume of fluid that passed through the sample. Permeability reached a steady state after 125 cm$^3$ of fluid flow. Ca$^{2+}$ reached a steady state level after about 150 cm$^3$ of fluid flow, while Mg$^{2+}$ continued to show variation until 175 cm$^3$ of fluid had passed through the sample.

## PW Experiments

Figure 2a illustrates the general behavior of PW tests (i.e., those immediately following surface polishing). Permeability decayed during the first 50 hours of flow, after which it was relatively constant. The concentration of Ca$^{2+}$ and Mg$^{2+}$ in the fluid increased during the first 10 hours, was stable until roughly 25 hours, and then increased between 26 and 46 hours. Ca$^{2+}$ remained at approximately 4 x10$^{-4}$ mol/L, while Mg$^{2+}$ increased to about 5 x10$^{-4}$. The variation in Mg$^{2+}$

at about 70 hours may be due to transient supersaturation or to the presence of very fine particles within the fluid samples. These variations are probably not due to analytical error (note the agreement between separate samples at 70 and 72 hours). The increase in chemical concentrations from 26 to 46 hours may be a function of the lower flow rates after about 40 hours, since our fluid system introduces a flow rate dependence for chemical composition changes as discussed previously.

Scatter in the permeability data is primarily related to flow rate variations that were associated with the abrupt fluid
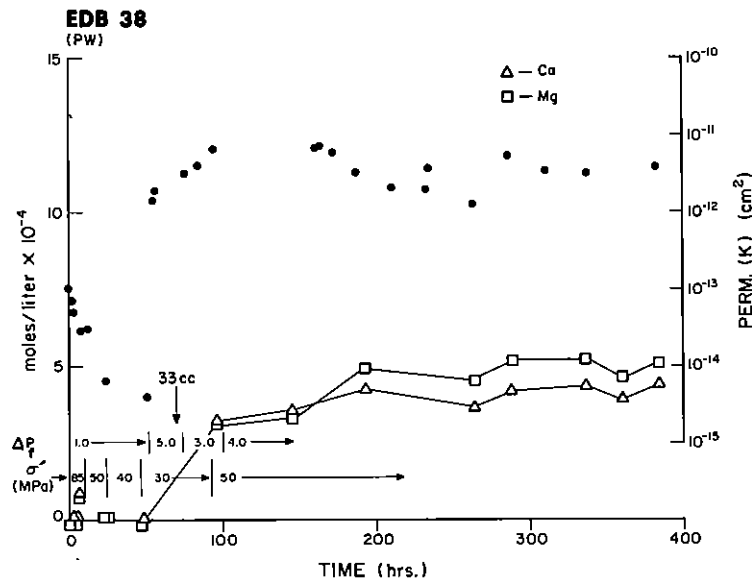
Fig. 3. Test EDB-38. Permeability (circles) and chemical concentration (squares and triangles) versus time for a PW experiment at high initial normal load are shown. Acid cleaning of the sample was done after polishing, as described in the text. Permeability decayed and chemical concentration increased during the initial hours, after which steady state values were reached. No long-term variation in chemical concentrations were observed after 100 to 150 hours of rock-fluid interaction. The steady state chemical values agree with those reached in 50 to 100 hours during shorter experiments. A fluid volume of 164 $cm^3$ had passed through the sample by 100 hours, and a total of 1283 $cm^3$ were forced through the joint in 346 hours. See text for discussion of low chemical concentrations during the first 50 hours.

pressure changes upon a change in flow direction through the sample. The flow rate was highest immediately after a change in flow direction and gradually decreased during a cycle to a constant rate, typically over a period of 3 to 4 hours. The change in flow rate was never more than a factor of 2, and permeability was calculated during the period of lowest flow rate for each cycle.

The chemical and permeability data from Figure 2a are replotted in Figure 2b versus cumulative volume flow through the sample. This is done here and in later figures in order to show the nature of variations in permeability and chemical composition as a function of the fluid volume that passed through the sample. Comparison of Figures 2a and 2b shows that 125 $cm^3$ of fluid passed through the sample within the first 24 hours. During this time, chemical concentrations increased while permeability decreased. Permeability showed little variation after 125 $cm^3$ of flow. Chemical concentrations showed a period of stability from 100 to 125 $cm^3$ and increased from 125 to 150 $cm^3$.

The question of whether the chemical concentrations reached in experiments such as EDB-39A are truly steady state values was addressed in a PW run lasting nearly 400 hours and shown in Figure 3. The data from EDB-38 indicate that chemical concentrations do not change significantly after about 150-200 hours. However, because of the high initial effective stress in this experiment ($\sigma' = 85$ MPa), and the resulting period of low permeability, chemical interaction between the joint and the bulk fluid was minimal before about 60 hours. That is, significant fluid flow did not begin until the permeability increased at about 60 hours. The rock-fluid interaction time required to reach steady state chemical composition for flow rates of $10^{-3}$-$10^{-4}$ $cm^3$/s is, therefore, more nearly 90-140 hours. A volume of 170 $cm^3$ had passed through the joint by 150 hours. As noted previously,

samples taken before at least 33 $cm^3$ of fluid had passed through the joint were diluted by unreacted fluid from reservoir B.

The permeability data of EDB-38 are complicated by changes in differential fluid pressure and effective normal stress. As was the case for the run shown in Figure 2, however, permeability decreased during the first 50-60 hours in EDB-38. The absolute permeability is lower in this run due to the higher normal stress. After $\sigma'$ was dropped to 30 MPa and $\Delta P_f$ was increased to 5.0 MPa at 50 hours, permeability increased to about $10^{-12}$ $cm^2$. Significant scatter in the permeability data was observed throughout this experiment, possibly as a result of fine particles being redistributed within the joint aperture during changes in flow direction.

*RF Experiments*

RF experiments were those in which the same sample was used in consecutive runs. These experiments were intended to assess the effects of polishing and to isolate the effects of normal load on changes in permeability and chemical concentration. For some RF experiments, the fluid system was refilled without changing $\sigma$, and thus these runs began without "initial loading." In order to avoid contamination with fluid from the preceding run, the fluid system was drained and refilled a total of three times between all consecutive runs.

The experiment shown in Figures 4a and 4b was designed to test the possibility that fine particles (insolubles or particles broken off the surfaces during loading) were responsible for long-term variations in permeability or fluid composition. The sample was first subjected to 40 MPa effective normal stress ($\sigma'$), and fluid was cycled through the joint for 7 hours. This was done at a high differential fluid pressure, 5.0 MPa, to facilitate flushing particles from the joint. Following the 7-
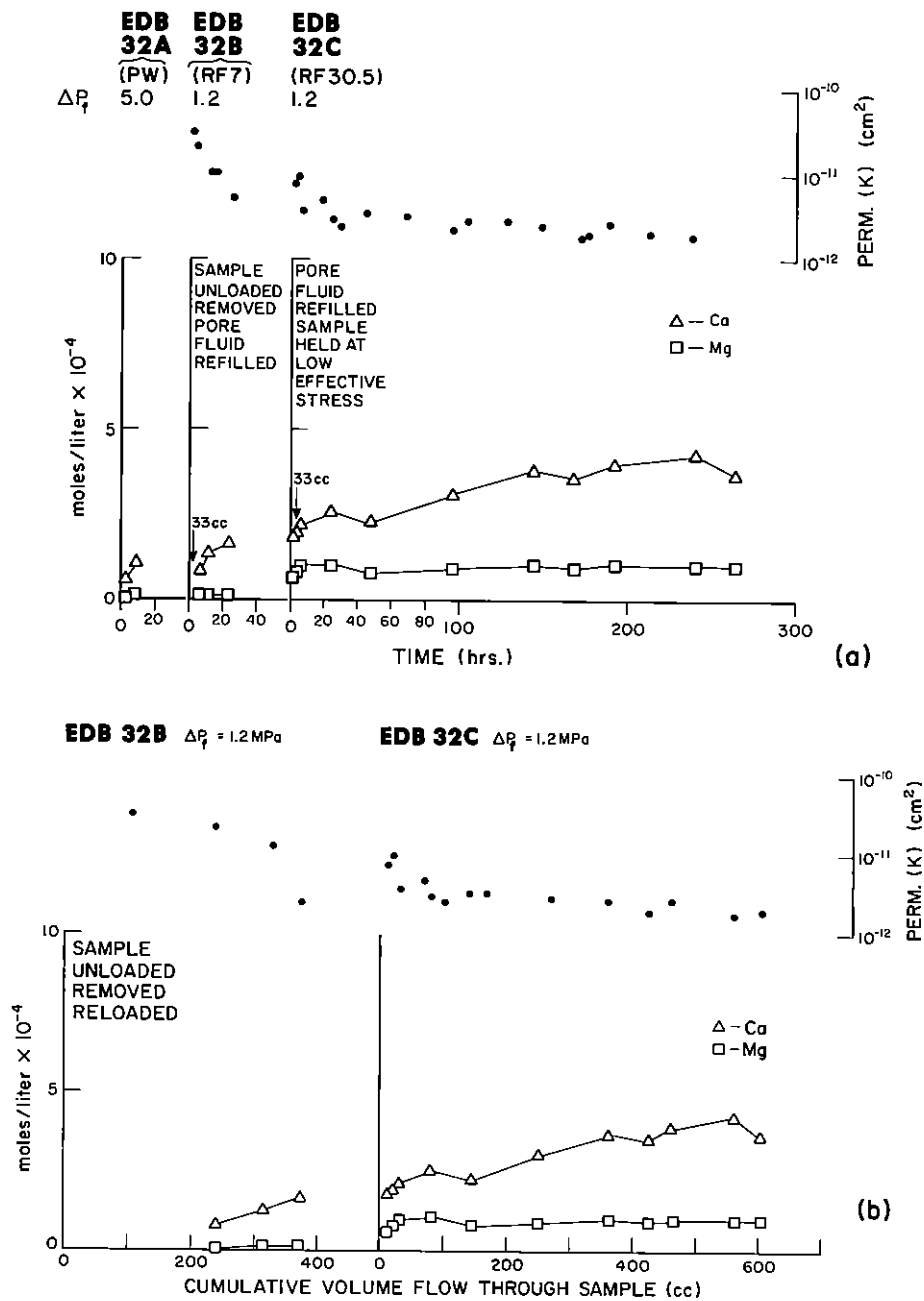
Fig. 4. Test EDB-32, a series of runs to test the possibility that fine particles caused permeability reduction and variations in chemical concentrations. The first two runs were designed to remove potential particles from the joint and pore fluid system. In spite of this, permeability reductions are observed in the third run along with chemical concentration increases. This argues against long-term permeability changes being due to clogging by particulates. The fluid in the $P_f$ system was not well mixed in the first two samples of the third run prior 33 cm$^3$ of flow. (a) Data for permeability and fluid composition are plotted as in Figure 2a. (b) The data from Figure 4a are plotted versus cumulative volume flow. Increases in Ca$^{2+}$ are observed in both runs after up to 300 cm$^3$ of fluid had passed through the sample.

hour run, the sample was removed from the vessel and the surfaces examined. The joint surfaces were cleaned with forced air to remove any loose particles; they were not subjected to additional polishing or interaction with water during this time. The sample was then rejacketed and inserted in the vessel, and the fluid system was flushed as described above. Confining pressure and axial load were reestablished with $P_f =$ 6.0 MPa and $\sigma' = 54$ MPa.

In the second run shown in Figure 4a (EDB-32B), chemical concentrations increased slightly and permeability decreased from 5 x10$^{-11}$ to 1 x10$^{-11}$ cm$^2$. Following 23.5 hours of fluid flow, the fluid pressure, confining pressure, and axial load were reduced to 0, 30, and 60 MPa, respectively. The fluid system was emptied and flushed as described earlier, and $\sigma'$ was raised to 50 MPa. The fluid pressure was increased before $P_c$ so as to avoid further surface damage associated with loading of the sample beyond its highest previous load. Fluid was then forced through the sample for 11 days. As shown in Figure 4a (32C), permeability decreased from 10$^{-11}$ to $\approx 5$ x 10$^{-12}$ cm$^2$ within 50 hours. The decrease in permeability was
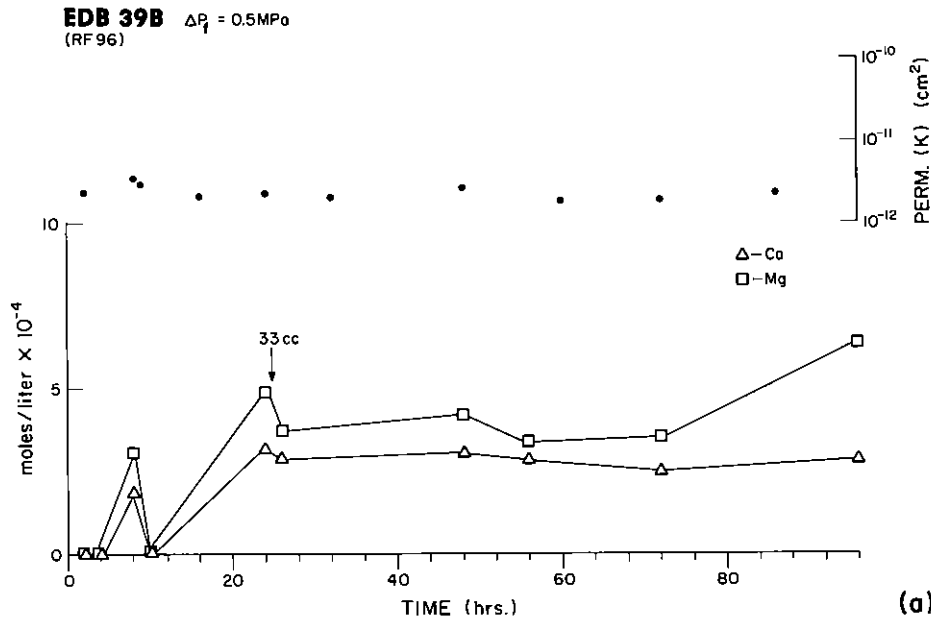
**EDB 39B** $\Delta P_f = 0.5 MPa$
(RF96)



(a)

Fig. 5. Test EDB-39B (RF96), an experiment run consecutively with 39A (Figure 2). The sample was not removed from the vessel between runs, and thus the surfaces were not repolished or otherwise treated between runs. The fluid was recharged at time zero while the sample was held at a constant effective stress. The chemical data before 33 cm$^3$ of flow occurred are complicated by dilution with unreacted fluid (see text). (a) Permeability (circles) and chemical concentration versus reaction time are shown. Note that permeability was not time dependent. (b) The data from Figure 5a are plotted versus flow volume. The fluid was not well mixed during the first four fluid samples. After 30 cm$^3$ of fluid flow the Ca$^{2+}$ values were relatively constant while those of Mg$^{2+}$ exhibited a larger variation.

fairly continuous across the unloading and fluid change between 32B and 32C. Chemical concentrations in 32C attained a steady state within 10-20 hours for Mg$^{2+}$ and 150 hours for Ca$^{2+}$. From Figure 4b, these times correspond to 40-50 cm$^3$ and 300 cm$^3$ of fluid flow, respectively. Note the rapid increase in chemical concentrations in run 32C, probably due to the lower flow rate as discussed earlier.

Figures 5 through 7 present data from a series of RF experiments. They follow EDB-39A (PW), which is shown in Figure 2. For these experiments, the sample was not removed

**EDB 39B** $\Delta P_f = 0.5 MPa$
(RF96)



(b)

CUMULATIVE VOLUME FLOW THROUGH SAMPLE (cc)

Fig. 5. (continued)

between runs, and the fluid system was flushed and refilled as described above. The joint surfaces were not repolished or otherwise altered between runs. These runs (39B, 39C, and 39D) are therefore similar to run 32C of Figure 4. Figures 5a and 6 show that a steady state chemical concentration was reached in 20-30 hours and that permeability did not show long-term variation. The chemical data in the early portion of these runs are complicated by dilution with unreacted fluid and, possibly, inadequate mixing within reservoir B; these data remain unexplained. The rapid approach to a steady state composition is consistent with the fluid being saturated as it exits the joint on its first pass through. Figures 5b and 6 show that a steady state chemical concentration was reached after 30-40 cm$^3$ of fluid flow.

In the run shown in Figure 5, $\sigma'$ was held constant between runs. Comparison with Figure 6, in which $\sigma'$ was cycled from 50 to 10 to 75 to 50 MPa between runs, shows that initial loading has no effect on the time history of permeability changes or on the steady state chemical concentrations. At 96 hours into the run shown in Figure 6 the effect of transient loading was tested; the load was cycled as follows (values in mega-pascals): $P_f$ to 2, $P_c$ to 18, $\sigma_1$ to 36, then $\sigma_1$ to 150 and $P_c$ to 75, and finally back to $\sigma_1$ of 120, $P_c$ of 60, and $P_f$ of 10. A chemical sample was taken at 95.5 hours to provide a reference for the transient loading. As seen in Figure 6, chemical concentrations and permeability following this stress cycle are not significantly different from those prior to loading. A fluid volume of 190 cm$^3$ passed through the sample by the end of EDB-39C.

Figures 7a and 7b show an RF experiment with a high flow rate, $2 \times 10^{-3}$ cm$^3$/s, and without initial loading (i.e., $\sigma'$ was held constant during fluid refilling). The data in Figure 7a indicate that permeability is not flow rate dependent; compare
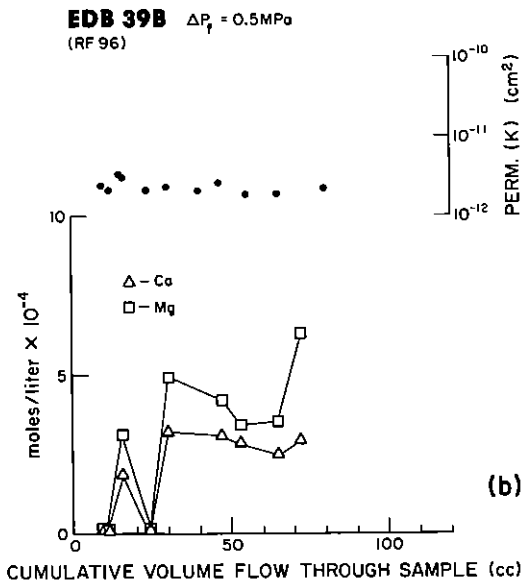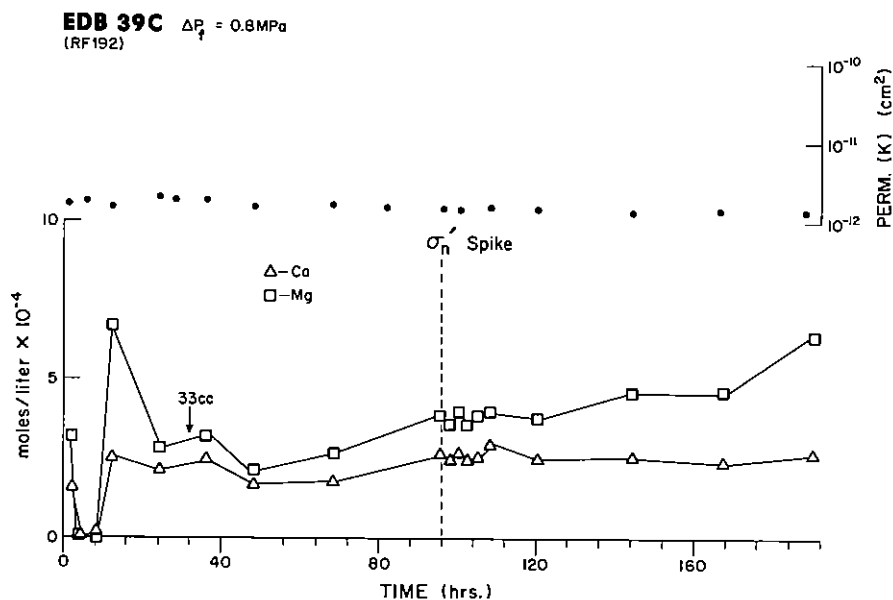
Fig. 6. Test EDB-39C (RF192). Normal load was varied from 10 MPa to 75 MPa while the pore fluid was being recharged. The chemical data before 33 cm³ of flow occurred are complicated by dilution with unreacted fluid. Permeability (circles) showed no long-term variation. A "spike" normal stress loading was input at 96 hours to test its effect on steady state permeability and chemical concentrations; see text for loading history. The pore fluid and permeability data just prior to the spike loading, at 95.5 hours, show that transient loading had no effect on either steady state permeability or pore fluid chemical composition.

Figures 7a, 5a and 6. The chemical concentrations in Figure 7a show less variability than previous ones, presumably as a result of greater mixing within the fluid reservoirs. The low chemical concentrations in this run (compare 39B and 39C at similar times) are consistent with the higher flow rate and shorter residence time of fluid within the joint.

Upon termination of a 16-day experiment (EDB-38), we examined a joint surface with a scanning electron microscope (SEM) in order to assess the changes in surface morphology that occurred during an experiment. For comparison, half of the surface was reground to reproduce its preexperiment condition. The preexperiment and postexperiment surfaces are shown in Figures 8a and 8b, respectively. The most striking difference is the loss of the sharp clean surfaces present before the experiment. In contrast, the reacted surface shows aligned etch pits along cleavage and a fine botryoidal phase (calcite? composition undetermined) within cavities. Figure 8c shows an enlargement of such a cavity on the reacted surface. Presumably, this material is the result of precipitation from a supersaturated solution. Similar features are not seen within cavities on the preexperiment side.

In summary, for PW runs, chemical concentrations increased during the initial 50 to 100 hours of rock-fluid interaction after which a steady state value was attained, ranging from $3 \times 10^{-4}$ to $4 \times 10^{-4}$ mol/L for $Ca^{2+}$ and $5 \times 10^{-4}$ to $6 \times 10^{-4}$ mol/L for $Mg^{2+}$. The permeability in PW runs decreased by about 1 order of magnitude during the initial 50 to 100 hours of fluid flow. After the initial decrease, permeability was $\approx 10^{-12}$ cm². In RF runs, steady state chemical concentrations ranged from $2 \times 10^{-4}$ to $3 \times 10^{-4}$ mol/L for $Ca^{2+}$ and $3 \times 10^{-4}$ to $5 \times 10^{-4}$ mol/L for $Mg^{2+}$. Permeability ranged between $1 \times 10^{-12}$ and $3 \times 10^{-12}$ cm² and was not time dependent.

## CALCULATION OF STEADY STATE CHEMICAL CONCENTRATIONS

For comparison with our chemical data, we calculated the solubility of Vermont marble in deionized water following the method of Garrels and Christ [1965, pp. 86-88]. In our experiments, the nominal pressure along the joint surface was 60 MPa, and the fluid pressure was 10 MPa. Such a state of nonhydrostatic stress is inherently one of nonequilibrium [e.g., Kamb, 1961; Li et al., 1966; Robin, 1978], however, a local equilibrium can exist. For example, within an adsorbed fluid layer, which exists within a contacting area, the local equilibrium solubility of solute within the fluid can be calculated on the basis of the local normal stress [Robin, 1978]. Alternatively, a local equilibrium could be calculated for an area far from a contact point for which the normal stress on the solid is simply that provided by the bulk fluid. In our system, the composition of the bulk fluid is controlled by the dissolution process at points of contact, the rate of diffusion/transfer of solute out of contact areas, and the kinetics of precipitation. We have chosen to include these affects in the steady state calculation by using a solid pressure, $P_{sol}$, of 60 MPa and a fluid pressure, $P_{fluid}$, of 10 MPa. This preserves some of the influence of higher normal stress at contact points while providing a conservative estimate of the bulk fluid composition. Ultimately, the concentrations within the bulk fluid depend on the rate of diffusion for solute components out of high-stress areas, and the kinetics of precipitation within lower-stressed regions. In the limit that precipitation in low-stress areas occurs instantaneously, we will overestimate the steady state concentrations (which will be those in equilibrium with a solid stressed by $P_{fluid}$). On the other hand, if precipitation is completely inhibited, we will

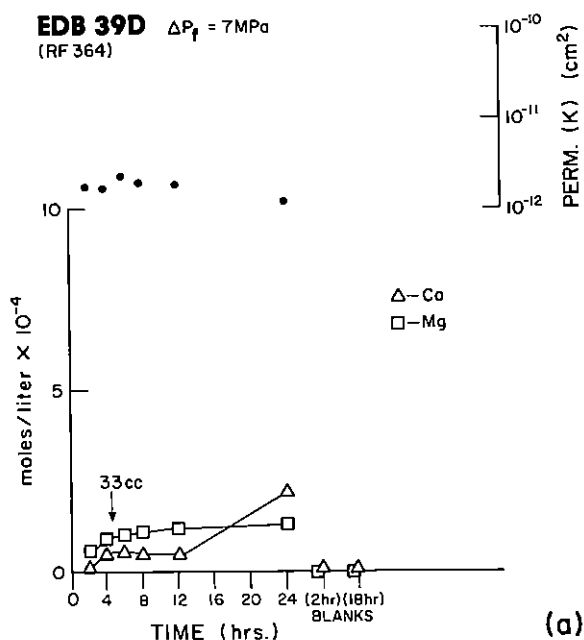**EDB 39D** $\Delta P_f$ = 7MPa
(RF 364)



Fig. 7. Test EDB-39D (RF364). Effective stress was held constant at the beginning of this run while the pore fluid system was flushed and refilled. (a) Comparison of this run with a run which started with an initial loading (Figure 6) shows that initial loading during RF runs did not have a significant effect on the time dependence of permeability (circles) or the steady state pore fluid chemical concentrations. The blanks shown to the right of the 24-hour sample were background chemical levels in the pore fluid system, without the rock sample, at the end of the series of four runs lasting a total of 398 hours. (b). The data from Figure 7a are plotted versus flow volume. The lower chemical concentrations compared with other RF runs are consistent with lower fluid residence times in the joint; see text for further discussion.

underestimate the steady state concentrations (which will be those in equilibrium with the highest-stress regions).

The deionized water used in our experiments was in equilibrium with atmospheric $P_{CO_2}$ before being pumped into

the vessel, and thus the $pH$ and the total dissolved carbonate in the water at the beginning of an experiment were 5.6 and $10^{-4.92}$ mol/L, respectively. These values enter into the equilibrium calculation through dissociation reactions for $H_2O$, $HCO_3^-$, and $H_2CO_3$. Because the fluid was sealed from atmosphere during a run, $pH$ and $P_{CO_2}$ varied as the marble-water reaction proceeded. We did not measure the $pH$ of the fluid samples collected during the experiments due to the difficulty in making such a measurement on a small aliquot of unbuffered solution. The $pH$ at steady state can be calculated on the basis of carbonate mass balance and electrical neutrality during dissolution [see *Garrels and Christ*, 1965, chapter 3, case 5].

The solid phases of the rock considered directly in the calculation, via a dissolution reaction and equilibrium constant, were calcite and dolomite. The calcite and dolomite dissolution reactions are

$$CaCO_3 = Ca^{2+} + CO_3^{2-}$$

and

$$(Ca_{0.565}Mg_{0.435})CO_3 = (0.565)Ca^{2+} + (0.435)Mg^{2+} + CO_3^{2-}$$
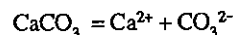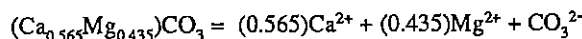
Other minor phases in the rock influence the equilibrium through common ion and speciation effects and were therefore considered in a term for the ionic strength of the solution and activity coefficients. The effect of pressure on the equilibrium constants for reactions involving carbonic acid, $H_2CO_3$, bicarbonate, $HCO_3$, and $H_2O$ was calculated using a standard relation [cf. *Broecker and Oversby*, 1971]:

$$\left[\frac{d(\ln K_{eq})}{dP}\right]_T = -\frac{\Delta V^o}{RT} \tag{1}$$

where $V^o$ represents the molal volumes for product and reactant species at standard state, $K_{eq}$ is the equilibrium constant, and $R, P$, and $T$ are the universal gas constant, pressure, and temperature, respectively.

Equilibrium constants for the calcite and dolomite dissolution reactions are $10^{-8.48}$ and $10^{-8.0}$, respectively, at
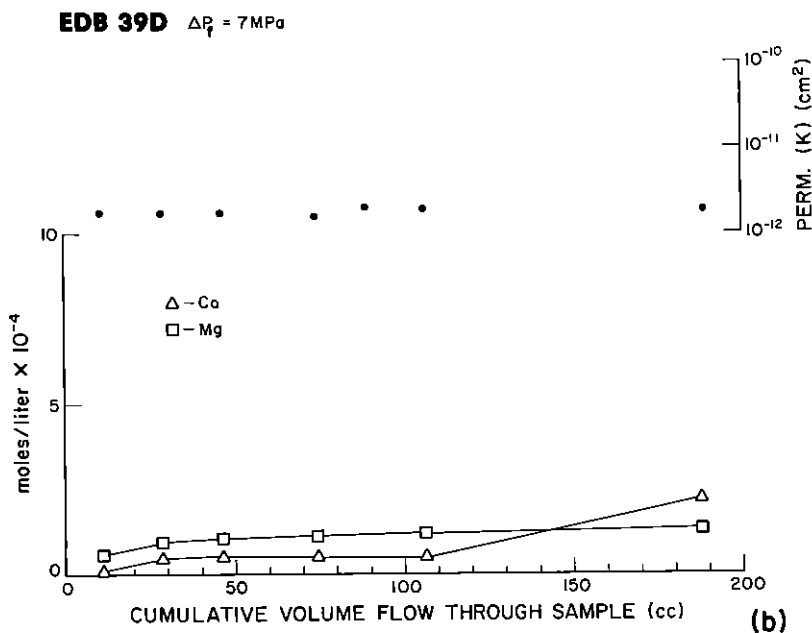
**EDB 39D** $\Delta P_f$ = 7MPa



Fig. 7. (continued)

Fig. 8a. Prerun surface. The scale bar at lower left is 20 μm. Note the sharp clean surfaces in the prerun photo and etched/pitted surfaces on the postrun photo. Precipitation features are visible in the cavities of the postrun side.



Fig. 8b. Postrun surface.



Fig. 8c. Closeup view of the postrun surface as in Figure 8b. The scale bar at lower left is 10 μm. Note the precipitation features in cavities.

Fig. 8. SEM photographs of surfaces from test EDB-38, comparing 400-grit surfaces before and after a 16-day run.

0.1 MPa (1 atm) and 25°C [*Plummer and Busenberg*, 1982; *Plummer and Mackenzie*, 1974]. We derived a pressure dependence for these equilibrium constants by considering the solid and fluid components separately in a relation similar to that given in (1).

$$\frac{K_{eq}^{P'}}{K_{eq}^{P_1}} = \exp\left[-\frac{(P_{fluid}-P_1)\,\Sigma v_i\,V_i^{aq}+(P_{sol}-P_1)\Sigma v_i V_i^{s}}{RT}\right] \quad (2)$$

Here, $K_{eq}^{P_1}$ is the 1 atm equilibrium constant, $K_{eq}^{P'}$ is the equilibrium constant at $P_{sol}$ and $P_{fluid}$, $v_i$ are the stoichiometric coefficients of species $i$ in the balanced reaction, and $V_i^{aq}$ and $V_i^{s}$ are the partial molal volumes of the aqueous and solid species, respectively. The only difference between (1) and (2) is in considering pressure effects on $\Delta V^o$ for solid and aqueous species separately. For a solid pressure of 60 MPa and a fluid pressure of 10 MPa, (2) yields $K_{eq}^{P'} = 10^{-8.26}$ for calcite dissolution and $K_{eq}^{P'} = 10^{-7.8}$ for dolomite dissolution (partial molal volume data from *Althoff* [1977], *Millero* [1969], and *Millero and Berner* [1972]).

We solve for the steady state concentrations by relating the variables and equilibrium constants from each dissolution reaction in equations for electrical neutrality and carbonate mass balance, first ignoring differences between molalities and activities and then considering such differences by successive approximation. The activity coefficients were calculated using the Debye-Huckel equation and an ionic strength of $5.58 \times 10^{-3}$. Ionic strength was calculated with data derived from direct measurements of metal cation concentrations and calculated values (for C-O-H species). After correcting for activities we find $[Ca^{2+}] = 3.90 \times 10^{-5}$ mol/L and $[Mg^{2+}] = 4.30 \times 10^{-4}$ mol/L, at 60 MPa solid pressure and 10 MPa fluid pressure. Measured concentrations in the solutions were $3 \times 10^{-4}$ to $5 \times 10^{-4}$ mol/L for $Ca^{2+}$, or 10 times the calculated value, and $5 \times 10^{-4}$ to $6 \times 10^{-4}$ mol/L for $Mg^{2+}$, or within a factor of 2.

## DISCUSSION

Joint surfaces not etched by previous reaction with water (PW tests) exhibited an initial permeability decay and reached steady state permeabilities of about $10^{-12}$ cm². Tests using samples that had undergone prior interaction with water (RF tests) did not show permeability changes, except for 32C, which was subject to only 31 hours of interaction. In both PW and RF experiments the concentrations of $Ca^{2+}$ and $Mg^{2+}$ in the fluid were supersaturated with respect to theoretical values. Cycling of the effective normal load at time zero and during chemical steady state did not have a significant effect on the subsequent steady state chemical composition or permeability.

*Permeability Data*

In our experiments, long-term permeability reduction occurred only during the first run after polishing. Permeability reduction may be attributed to permanent mechanical deformation upon initial loading as indicated by the work of *Brown and Scholz* [1985, 1986]. However, the permanent deformation in Brown and Scholz's experiments took place almost instantaneously upon loading. Because this type of behavior would have occurred long before permeability measurements commenced, we reject this process as being responsible for the reduction in permeability during PW runs.

Alternative hypotheses to explain the observed reduction in permeability include (1) deposition of material within flow channels and (2) preferential dissolution of material at, and/or stress-corrosion cracking of, contact points and thus a reduction in hydraulic aperture. Each of these hypotheses may be subdivided. Flow channels may be clogged by fine particles or by chemical precipitation. For the second possibility, two models for asperity degradation via pressure solution have been proposed (1) the *Weyl* [1959] model in which dissolution takes place along an adsorbed film between a solid-solid contact and (2) the *Bathurst* [1958] model in which dissolution occurs at the margin of contact areas.

We reject the hypothesis that clogging of flow channels caused permeability reduction for the following reasons. Precipitation is known to have occurred in RF experiments (Figure 8c), however, permeability reduction was observed only in PW experiments. In addition, permeability decreased during the initial stages of PW experiments, while chemical concentrations were increasing within the fluid, and thus while net dissolution was exceeding net precipitation. Therefore it does not seem likely that precipitation was a principal cause of permeability reduction. As for the possibility of clogging of flow channels by fine particles, recall that the flow rate decreased during the initial portion of each flow cycle following a change in flow direction. One possible explanation for this observation is that very fine particles (insolubles or particles generated via fracture of contacting asperities) clogged the smaller flow channels and were dislodged upon a change in flow direction. The possibility that fine particles influenced longer-term permeability reduction was tested in runs EDB-32A through EDB-32C (Figure 4). In these tests, two separate attempts were made to clean or flush particles from the joint surface, but permeability reduction was observed following each attempt. This indicates that long-term permeability reduction did not occur by clogging of flow channels.

We are left with the hypothesis that asperities, which hold the joint open under normal load, collapse via physicochemical dissolution and material removal. Stress-corrosion cracking may also contribute to asperity degradation, however, this cannot explain the observed increases in fluid chemical composition. Physicochemical dissolution is consistent with the basic time dependence of permeability in PW experiments. However, instead of only mechanical damage, our experiments suggest that both mechanical and chemical processes operate to produce a time dependent joint closure during the first application of normal load in the presence of a solvent. The lack of permeability reduction in RF experiments is consistent with degradation of large weak asperities left by polishing during the first chemical interaction under load.

As a test of the time dependent closure model we calculated permeability changes from our chemical data using the cubic law for permeability of a joint [e.g., *Gangi*, 1978; *Kranz et al.*, 1979]. The cubic law is applicable to flow between smooth parallel plates of aperture $d$ and is given by $q = (d^3/12\mu)\,(dP/dL)$, where $\mu$ is the fluid viscosity, $dP/dL$ is the pressure gradient, and $q$ is the volume flow rate per plate width. While our joint surfaces are not smooth, but contact at discrete points, the cubic law adequately describes fluid flow through joints under a variety of conditions [cf. *Witherspoon et al.*, 1980].

If dissolution occurs preferentially at contact points, the hydraulic aperture of a joint will decrease as the chemical concentrations in the fluid increase. On the other hand, if dissolution occurs within flow channels, permeability may increase as the chemical composition of the fluid increases. Our PW experiments indicate that permeability decreases as chemical concentrations increase. To evaluate this relationship, we derived changes in joint aperture from the chemical data by calculating the volume of solid material, $dV^s$, necessary to produce the observed concentration change within the fluid, $dC$, during a given time interval:

$$dV^s = V^f\,\Sigma(dC_i\,V_i^o)$$

where $V^f$ is the volume of fluid within the pore fluid system during a given time interval and $V_i^o$ is the molar volume of chemical species $i$ within the rock. A change in joint aperture, $d$, was obtained from $dV^s$ by assuming dissolution occurred over an area $A$:

$$d = dV^s/A$$

The calculated and measured permeability changes for two PW type experiments (EDB-32 in Figure 4 and EDB-39A in Figure 2) are given in Figure 9. Permeability changes were calculated using the nominal surface area of the joint and a lesser area which fit the permeability change; the latter areas should be considered as ± 3%. The calculated permeability was arbitrarily set equal to the measured permeability at time zero to facilitate comparison. Figure 9 shows that using the nominal surface area to calculate the aperture change underestimates the permeability change. However, if dissolution is assumed to occur over a restricted portion of the joint surface, the permeability reduction can be fit. This is consistent with preferential dissolution at contact points, although the real area of contact would probably be closer to 20-25% of the nominal surface area [cf. *Brown and Scholz*, 1986]. Our data are therefore consistent with pressure solution, however, we are unable to distinguish between the models proposed by *Bathurst* [1958] and *Weyl* [1959].

*Chemical Data*

The steady state chemical concentrations in our experiments were supersaturated with respect to the calculated $Ca^{2+}$ values and roughly equal to calculated $Mg^{2+}$ values. Possible reasons for this are (1) the steady state calculation is based on the nominal normal stress across the joint, whereas higher stresses occur at contact points; (2) precipitation kinetics are generally more sluggish than dissolution kinetics; or (3) initial surface damage during loading creates large surface areas on highly strained particles which dissolve readily and are poor sites for precipitation.

In calculating a pressure dependence for the equilibrium constants we used the nominal normal stress on the joint of 60 MPa. The stress at contact points is, however, substantially higher. Higher chemical concentrations in the bulk fluid would result from the higher solid pressure if precipitation in low-stress areas were inhibited. In the limit that precipitation was completely inhibited, the fluid would become saturated with respect to the highest-stressed areas. In the other extreme (no kinetic barriers to precipitation), the bulk fluid would be at equilibrium with respect to a hydrostatically stressed solid under pressure $P_{fluid}$. The end-member cases for local equilibrium provide bounds on the

## EDB-32B & C



o Measured K
● K(Nominal Area)
X K(45% Nominal Area)

## EDB-39A



o Measured K
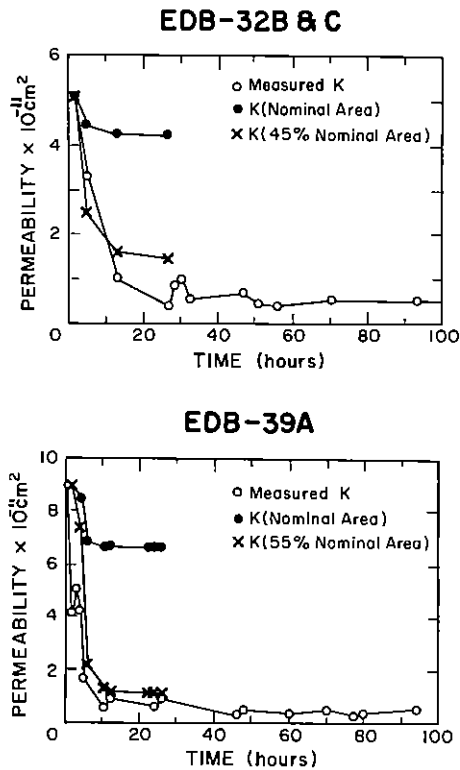● K(Nominal Area)
X K(55% Nominal Area)

Fig. 9. Predicted and measured permeability changes for two PW type experiments. Permeability changes were derived from changes in chemical concentration by assuming a surface area over which material was removed and using the cubic law for flow through joints. The values estimated using the nominal surface area underpredict the measured permeability reduction. If dissolution is assumed to occur preferentially over a restricted portion of the surface, the permeability changes can be predicted from changes in the chemical composition of the fluid.

range of steady state concentrations possible within the bulk fluid. Using (1) and repeating the calculation given previously, we find $[Ca^{2+}] = 3.142 \times 10^{-5}$ and $[Mg^{2+}] = 3.89 \times 10^{-4}$ mol/L for $P_{fluid} = P_{sol} = 10$ MPa. For the highest-stressed areas, we can take 10% of the nominal surface area as a minimum real area of contact [cf. *Brown and Scholz*, 1986], which gives $P_{sol} = 600$ MPa. Moreover, if a load-bearing fluid layer exists within contact areas as has been suggested by *Weyl* [1959], *de Boer* [1977], and *Rutter* [1983], $P_{fluid}$ would equal $P_{sol}$ within the contact areas. Under these conditions, we find $[Ca^{2+}] = 1.30 \times 10^{-3}$ and $[Mg^{2+}] = 7.82 \times 10^{-3}$ mol/L for $P_{fluid} = P_{sol} = 600$ MPa. In our solutions $[Ca^{2+}] \approx 3 \times 10^{-4}$ and $[Mg^{2+}] \approx 4 \times 10^{-4}$ mol/L. These values are clearly in the range defined by the extremes in pressure/precipitation kinetics.

Locally higher normal stresses at grain-to-grain contacts will aid in the dissolution process; however, to sustain steady state supersaturation, precipitation must also be inhibited. Possibly, precipitation in low-normal-stress areas is inhibited by shear stresses or high strain energy around contact points. Sluggish precipitation kinetics could also cause supersaturation. The fact that our measured $Mg^{2+}$ concentrations approximately match the values for $P_{sol} = 60$ MPa, whereas the $Ca^{2+}$ is supersaturated, is consistent with precipitation being inhibited more effectively for pure calcite than for an Mg-rich phase. That is, equilibrium with pure

calcite and dolomite that is more Mg-rich than $Ca_{0.565}Mg_{0.435}CO_3$ would result in higher $Ca^{2+}$ values than those calculated above. The magnitude of the observed supersaturation, however, cannot be explained by this mechanism. The Mg/Ca ratio observed in our solutions could be explained if an Mg-bearing carbonate (magnesian calcite, dolomite) was the sole precipitating phase.

### SUMMARY AND CONCLUSIONS

Two types of experiments were performed to evaluate the relationship between permeability changes within an artificial joint and chemical concentrations within a fluid forced through the joint. The main difference in these experiments was in the treatment of the surfaces prior to a run; in one case the surfaces were polished just prior to an experiment, and in the other a sample was used in consecutive experiments without additional polishing or surface treatment between runs.

Permeability decreasesd during the initial stages of experiments following surface polishing. In the consecutively run experiments, permeability was not time dependent. The chemical composition of the fluid increased during the initial stages of both types of experiments, and the steady state values were supersaturated with respect to calculated values using a solid pressure of 60 MPa and a fluid pressure of 10 MPa. Possible explanations for the supersaturated solutions include the locally higher stresses at contact points, slow precipitation kinetics, and the effects of surface damage induced during polishing. We suggest that higher stress at contact points promotes pressure solution which together with precipitation inhibition in lower-stressed areas results in the observed concentrations.

Depending upon whether dissolution occurs within flow channels or at load-bearing contact areas, the permeability of a fracture may increase or decrease as a fluid flowing through it becomes saturated. Our PW experiments show decreases in permeability as chemical concentrations in the fluids increase. Such decreases are consistent with dissolution of load-bearing contact points and subsequent reduction in hydraulic aperture. After a chemical steady state was achieved, no long-term variations in permeability were observed. Permeability changes calculated from changes in chemical concentrations overpredict measured permeability changes if we assume that material was removed evenly over the nominal surface area. This suggests that initial dissolution and material loss occurs over a fraction of the nominal surface area, at contact points. The idea that pressure solution facilitates the removal of material at contact points is consistent with the observed permeability reductions.

## REFERENCES

Althoff, P. L., Structural refinements of dolomite and a magnesian calcite and implications for dolomite formation in the marine environment, *Am. Mineral.*, *62*, 772-783, 1977.

Bathurst, R. G. C., Diagenetic fabrics in some British Dinantian limestones, *Liverpool Manchester Geol. J.*, 2, 11-36, 1958.

Broecker, W. S., and V. M. Oversby, *Chemical Equilibria in the Earth*, p. 303, McGraw-Hill, New York, 1971.

Brown, S. R., and C. H. Scholz, Closure of random elastic surfaces in contact, *J. Geophys. Res.*, *90*, 5531-5545, 1985.

Brown, S. R., and C. H. Scholz, Closure of rock joints, *J. Geophys. Res.*, *91*, 4939-4948, 1986.

Chave, K. E., and R. F. Schmalz, Carbonate-seawater interactions, *Geochim. Cosmochim. Acta*, *30*, 1037-1048, 1966.

Chou, L., and R. Wollast, Study of the weathering of albite at room temperature and pressure with a fluidized bed reactor, *Geochim. Cosmochim. Acta*, *48*, 2205-2217, 1984.

de Boer, R. B., Pressure solution: Theory and experiments, *Tectonophysics*, *39*, 287-301, 1977.

Engelder, T., The role of pore water circulation during the deformation of foreland fold and thrust belts, *J. Geophys. Res.*, *89*, 4319-4325, 1984.

Etheridge, M. A., V. J. Wall, S. F. Cox, and R. H. Vernon, High fluid pressures during regional metamorphism and deformation: Implications for mass transport and deformation mechanisms, *J. Geophys. Res.*, *89*, 4344-4358, 1984.

Fyfe, W. S., N. J. Price, and A. B. Thompson, *Fluids in the Earth's Crust*, 383 pp., Elsevier, New York, 1978.

Gangi, A. F., Variations of whole and fractured porous rock permeability with confining pressure, *Int. J. Rock Mech. Min. Sci.*, *15*, 249-257, 1978.

Garrels, R. M., and C. L. Christ, *Solutions, Minerals, and Equilibria*, Freeman, Cooper, pp. 74-92, San Francisco, Calif., 1965.

Holdren, G. R., and R. A. Berner, Mechanism of feldspar weathering, I, Experimental studies, *Geochim. Cosmochim. Acta*, *43*, 1161-1171, 1979.

Iwai, K., Fundamental studies of fluid flow through a single fracture, Ph.D. thesis, Stanford Univ., Stanford, Calif. 1976.

Kamb, W. B., The thermodynamic theory of nonhydrostatically stressed solids, *J. Geophys. Res.*, *66*, 259-271, 1961.

Kranz, R. L., and J. D. Blacic, Permeability changes during time-dependent deformation of silicate rock, *Geophys. Res. Lett.*, *11*, 975-978, 1984.

Kranz, R. L., A. D. Frankel, T. Engelder, and C. H. Scholz, The permeability of whole and jointed Barre granite, *Int. J. Rock Mech. Min. Sci.*, *16*, 225-234, 1979.

Li, J. C. M., R. A. Oriani, and L. S. Darken, The thermodynamics of stressed solids, *Z. Phys. Chem.*, *49* (3/4), 271-290, 1966.

McClay, K. R., Pressure solution and Coble creep in rocks and minerals: A review, *J. Geol. Soc. London*, *134*, 57-75, 1977.

Millero, F. J., The partial molal volume of ions in seawater, *Limnol. Oceanogr.*, *14*, 376-385, 1969.

Millero, F. J., and R. A. Berner, Effect of pressure on carbonate equilibria in seawater, *Geochim. Cosmochim. Acta*, *36*, 92-98, 1972.

Moore, D. E., C. A. Morrow, and J. D. Byerlee, Chemical reactions accompanying fluid flow through granite held in a temperature gradient, *Geochim. Cosmochim. Acta*, *47*, 445-453, 1983.

Morrow C., D. Lockner, D. Moore, and J. D. Byerlee, Permeability of granite in a temperature gradient, *J. Geophys. Res.*, *86*, 3002-3008, 1981.

Plummer, L. N., and F. T. Mackenzie, Predicting mineral solubility from rate data: Application to the dissolution of magnesian calcites, *Am. J. Sci.*, *274*, 61-83, 1974.

Plummer, L. N., and E. Busenberg, The solubilities of calcite, aragonite and vaterite in $CO_2$-$H_2O$ solutions between 0 and 90°C, and an evaluation of the aqueous model for the system $CaCO_3$-$CO_2$-$H_2O$, *Geochim. Cosmochim. Acta*, *46*, 1011-1040, 1982.

Potter, J. M., W. E. Dibble, and A. Nur, Effects of temperature and solution composition on the permeability of St. Peters sandstone —Role of iron (III), *J. Petroleum Tech.*, May, 905-907, 1981.

Robin, P.-Y. F., Pressure solution at grain-to-grain contacts, *Geochim. Cosmochim. Acta*, *42*, 1383-1389, 1978.

Rutter, E. H., Pressure solution in nature, theory, and experiment, *J. Geol. Soc. London*, *140*, 725-740, 1983.

Sass, E., J. W. Morse, and F. J. Millero, Dependence of the values of calcite and aragonite thermodynamic solubility products on ionic models, *Am. J. Sci.*, *283*, 218-229, 1983.

Summers, R., K. Winkler, and J. D. Byerlee, Permeability changes during the flow of water through Westerly granite at temperatures of 100-400°C, *J. Geophys. Res.*, *83*, 339-344, 1978.

Tada, R., and R. Siever, Experimental knife-edge pressure solution of halite, *Geochim. Cosmochim. Acta*, *50*, 29-36, 1986.

Walter, L. M., and J. W. Morse, Magnesian calcite stabilities: A reevaluation, *Geochim Cosmochim. Acta*, *48*, 1059-1069, 1984.

Weyl, P. K., Pressure solution and the force of crystallization—A phenomenological theory, *J. Geophys. Res.*, *64*, 2001-2025, 1959.

Witherspoon, P. A., J. S. Y. Wang, K. Iwai, and J. E. Gale, Validity of the cubic law for fluid flow in a deformable rock fracture, *Water Resour. Res.*, *16*, 1016-1024, 1980.

Wright, T. O., and L. B. Platt, Pressure dissolution and cleavage in the Martinsburg Shale, *Am. J. Sci.*, *282*, 122-135, 1982.

T. Engelder, Department of Geosciences, Pennsylvania State University, University Park, PA 16802.

C. Marone and J. Rubenstone, Lamont-Doherty Geological Observatory, Columbia University, Palisades, NY 10964.